Journal of Thermal Analysis and Calorimetry (2022) 147:2749–2759
https://doi.org/10.1007/s10973-021-10568-x

Cattaneo–Christov heat flux theory on transverse MHD Oldroyd-B liquid over nonlinear stretched flow

K. Venkata Ramana[1] · K. Gangadhar[2] · T. Kannan[3] · Ali J. Chamkha[4,5]

Received: 20 June 2020 / Accepted: 8 January 2021 / Published online: 15 February 2021

Abstract

A hydromagnetic transverse flow of an Oldroyd-B-type liquid with a heat flux of the Cattaneo–Christov model with variable thickness has been analyzed. Consider additional impacts of thermal conductivity as well as heat generation. Governing equations were transmitted into a set of nonlinear ordinary differential equations using similarity conversion, and then, numerical solution was evaluated using the procedure Runge–Kutta–Fehlberg. The physical response related to velocity and temperature is investigated computationally. The outcomes also show that the momentum boundary-layer thickness increases the values of magnetic field strength, but the reverse trend is observed for the thermal boundary layer. Impacts of retardation and relaxation time effects are quite the opposite of the temperature field. The obtained computations are useful in transport phenomena which are involving hydromagnetic rheological fluids.

Keywords Oldroyd-B fluid · Thermal conductivity of temperature · MHD · Heat source/sink · Non-Fourier's heat flux

List of symbols

B_0	Magnetic field strength (N m^{-1} A^{-1})
B	Applied magnetic field (N m^{-1} A^{-1})
b	Positive constant (s^{-1})
U_w	Stretching velocity (ms^{-1})
T_w	Temperature of fluid at the wall (K)
T_∞	Ambient fluid temperature (K)
x_1, x_2	Coordinate axis (m)
T	Temperature (K)
n	Power law index
G	Dimensionless velocity
M	Magnetic parameter
C_p	Heat capacity (J kg^{-1} K)
U_0	Reference velocity (s^{-1})
k_∞	Ambient fluid thermal conductivity
Q	Heat generation/absorption coefficient (J kg^{-3} K^{-1} s^{-1})
k	Thermal conductivity (Wm^{-1} K^{-1})
Pr	Prandtl number
q_w	Wall heat flux (Wm^{-2})
Cf_{x_1}	Skin friction coefficient
Nu_{x_1}	Local Nusselt number
Re_{x_1}	Local Reynolds number

Greek symbols

ξ_1, ξ_2	Velocity components (ms^{-1})
ν	Kinematic viscosity (m^2 s^{-1})
λ_1	Relaxation time (s)
λ_2	Retardation time (s)
η	Similarity variable
τ_w	Wall shear stress
β_1, β_2	Deborah numbers
δ	Heat generation/absorption parameter
Θ	Dimensionless temperature
γ	Thermal relaxation parameter

✉ Ali J. Chamkha
alichamkha@duytan.edu.vn

K. Venkata Ramana
ramana.may@gmail.com

K. Gangadhar
kgangadharmaths@gmail.com

T. Kannan
krishnakannan108@gmail.com

[1] Department of Mathematics, Vignan's Lara Institute of Technology and Science, Vadlamudi, Guntur, Andhra Pradesh 522213, India

[2] Department of Mathematics, Acharya Nagarjuna University, Ongole, Andhra Pradesh 523001, India

[3] Department of Mathematics, School of Humanities and Sciences, SASTRA Deemed University, Thanjavur, TN, India

[4] Institute of Research and Development, Duy Tan University, Da Nang 550000, Vietnam

[5] Institute of Theoretical and Applied Research (ITAR), Duy Tan University, Hanoi 100000, Vietnam

ρ Density of the fluid (kg m^{-3})
σ Electrical conductivity (Sm^{-1})

Subscripts

∞ Condition at the free stream
w Condition at the wall/surface

Introduction

Using the physical theory of heat and fluid flow, the rapid existence of force and free convection is known as mixed convection. The buoyancy parameter is defined as the impact of forced and free flows. Many researchers in heat flow are paying attention to areas like system cooling and power transmission. Fluids do not follow Newton's law of viscosity in engineering and industrial mechanisms, and these fluids' nature was non-Newtonian such as fluid cleansers, ketchup, polymer, shampoos, apple sauce, paper pulp, and paints. A big challenge for mathematicians is to obtain an exact solution for the related nonlinear equations while dealing with non-Newtonian fluids (Hayat and Nadeem [1], Ellahi et al. [2]). In these situations, so many researchers have committed their research to non-Newtonian fluids due to their significant utilizations. Various authors, similar to Elbashbeshy et al. [3], Nadeem et al. [4], and Shenoy [5] authors, have invented diverse non-Newtonian models. Many models have been analyzed and studied for non-Newtonian fluids in the preceding decades. Navier–Stokes equations cannot represent the real conduct of these materials. In those fluids, Oldroyd-B, one type of fluid, is used in this paper. This model is a most excellent fit for the exploration of shear-thickening and shear-thinning impacts.

It is greatly acknowledged that in the circumstances comprising short times, maximal temperatures, or thermal gradients near absolute zero, Fourier's heat diffusion concept becomes imprecise and non-Fourier consequence becomes decisive in characterizing the diffusion mechanism and anticipating temperature distribution. Practical aspects where deviance from the Fourier's model turns noteworthy may be encountered, for example, in microelectronic materials including IC clips, heating of laser pulse with high heat flux or concise duration for hardening of semiconductors, impulse drying, and laser surgery in biomedical engineering. In our nature, heat transfer available by the temperature variances among two bodies at distinct temperatures has a vital role. Accordingly, that heat transfer occurrence via Fourier's law of heat conduction [6] was focused on by scientists and researchers, and it gives a source to the study of heat transfer aspect. A primary suspension is felt directly in the whole material. To rectify the above trouble, a thermal relaxation time, which allows the transmission of heat from beginning to end, spreads heat waves with limited speed, added by Cattaneo [7]. After that, by assuming thermal relaxation time together, Oldroyd's upper-convected derivatives to the above inequality were solved by Christov [8]. Later, Straughan [9] analyzed this model in thermal convection flow. Tibullo and Zampoli [10] observed the similarity of the above problem to the incompressible fluid flows. Some attempts are made in this direction through [11–30] and many studies therein.

Magnetohydrodynamic (MHD) non-Newtonian or Newtonian fluid consists of many functions in various fields of engineering and technology. Fluids defined above are essential in tunable optical fiber filters, polymer industry, optical switches, metallurgy, optical granting, stretching of plastic materials, and optical modulators. Required product quality depends on stretching and cooling rates via drawing and that type of strips in an eclectically conducting fluid having certain features. Liquid and magnetic properties consist of only one fluid, which is magnetic Oldroyd-B fluid. By using a varying magnetic field, the fluid's physical characteristics can be changed. Khan et al. [31] deliberated Maxwell's influence, MHD on Jeffrey, Oldroyd-B fluids over the unsteady stretched surface. Mehmood et al. [32] assume the MHD flow of an Oldroyd-B fluid on a stretching wall in addition to the Newtonian heating effect. The influence of MHD in other related works are discussed in [33–48].

In cooling systems, the study of impacts of absorption or generation is most significant. In most physical situations, perfect modeling of internal heat absorption or generation was given by mathematical models. The impact of heat generation accounts for energy expression. Heat generation is a vital aspect in heat removal from nuclear fuel debris processes, storage of food kinds of stuff, disassociating fluids in packed-bed reactors, underground disposal of radioactive waste material, etc. In an inclined plate, the impacts of internal heat absorption or generation on the nanofluid flow were deliberated by Akilu and Narahari [49]. Ganga et al. [50] studied numerically and analytically the MHD flow of nanofluid over a vertical plate with heat absorption or generation and ohmic dissipation. Gangadhar et al. [51] analyzed and used spectral methods to be aware of the unsteady free convective flow of a nanofluid with heat generation properties.

Motivated by the above-mentioned studies and challenges, this analysis aims to recognize properties of Oldroyd-B fluid in MHD flow with Cattaneo–Christov heat flux over a nonlinear stretched sheet with variable thickness. Moreover, notice that shear-thinning/shear-thickening and typical stress impacts cannot be predicted by Oldroyd-B liquid. By using temperature-dependent thermal conductivity, properties of flow are explored. By using relevant parameters, the profile of velocity and temperature are analyzed. To our notice, such effort for the nonlinear stretched case is not obtained up till now. Moreover, the current challenge with the steady of the thermal conductivity case does not exist until now. This type of flow may have important applications in nuclear reactor cooling systems, biomedicine, electronics, glass fiber

production, hot rolling, food processing, and transportation. The mathematical model consisting of differential equations of the assumed study is developed in "Mathematical formulation" section. In "Numerical solution" section, the Runge–Kutta–Fehlberg method is used to solve the coupled set of ODEs. In "Results and discussion" section, the obtained results are discussed. We conclude and summarize this study in "Conclusions" section.

Mathematical formulation

Consider Oldroyd-B fluid flow in two-dimensional space over the stretchable and nonlinear surface at $x_2=0$. Along the surface, the variable x extends as well as fluid lines in the region $x_2 \geq 0$. The normal to the surface is $B(x_1)$ and strength of magnetic field $B(x) = B_0\left(x_1+b\right)^{\frac{n-1}{2}}$. $B(x_1)$ is non-dependent of time, so $Curl(E) = 0$. In the deficiency of surface charge density, $div(E)=0$. Thus, the external electric field is supposed to be insignificant. The surface stretches along with x_1-direction, and the velocity in this direction is $U_w = U_0(x_1+b)^n$, where $U_0(s^{-1})>0$ is the non-negative constant which portends the rate of stretching (see Fig. 1 for substantial construction of the problem). We considered a model by replacing classical Fourier's law of heat conduction with Cattaneo–Christov heat flux. Heat transfer properties are analyzed by using heat generation/absorption and thermal conductivity of temperature. Additionally, assume relation between ambient temperature T_∞ and wall temperature T_w as $T_w > T_\infty$. By using boundary-layer estimations ($O(x_1)=O(\xi_1)=1$, $O(x_2)=O(\xi_2)=\delta$), the governing equalities are given as follows [11]:

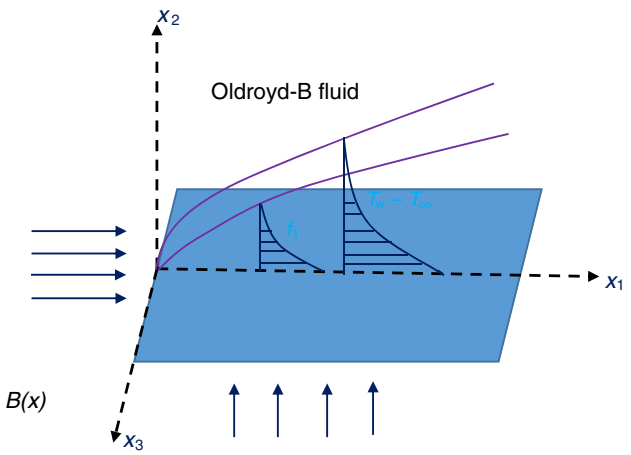

Fig. 1 Model configuration and geometry

$$\frac{\partial \xi_1}{\partial x_1} + \frac{\partial \xi_2}{\partial x_2} = 0, \tag{1}$$

$$\begin{aligned} &\xi_1\frac{\partial \xi_1}{\partial x_1} + \xi_2\frac{\partial \xi_1}{\partial x_2} \\ &+ \lambda_1\left(\xi_1^2\frac{\partial^2 \xi_1}{\partial x_1^2} + \xi_2^2\frac{\partial^2 \xi_2}{\partial x_2^2} + 2\xi_1\xi_2\frac{\partial^2 \xi_1}{\partial x_1 \partial x_2}\right) \\ &- \upsilon\lambda_2\left(\xi_1\frac{\partial^3 \xi_1}{\partial x_1 \partial x_2^2} + \xi_2\frac{\partial^3 \xi_1}{\partial x_2^3} - \frac{\partial \xi_1}{\partial x_1}\frac{\partial^2 \xi_1}{\partial x_2^2} - \frac{\partial \xi_1}{\partial x_2}\frac{\partial^2 \xi_2}{\partial x_2^2}\right) \\ &+ \frac{\sigma B_0^2}{\rho}\left(\xi_1 + \lambda_1\frac{\partial \xi_1}{\partial x_2}\right) = \upsilon\frac{\partial^2 \xi_1}{\partial x_2^2}, \end{aligned} \tag{2}$$

$$\rho c_p\, v\cdot\nabla T = -\nabla\cdot q + Q\left(T - T_\infty\right). \tag{3}$$

By using Cattaneo–Christov heat flux, we get

$$q + \tau_0\left(\frac{\partial q}{\partial t} - q\cdot\nabla v + v\cdot\nabla q + (\nabla\cdot v)q\right) = -k(T)\nabla T. \tag{4}$$

In the above equation, τ_0 denotes the heat flux-related relaxation time and $k(T)$ denotes the temperature thermal conductivity. By substituting the thermal relaxation parameter $\tau_0=0$ into Eq. (4), then it turned into classical Fourier's law, and fluid incompressibility declares that

$$\boldsymbol{q} + \tau_0\left(\frac{\partial q}{\partial t} + \boldsymbol{v}\,.\boldsymbol{\nabla q} - \boldsymbol{q}.\boldsymbol{\nabla v}\right) = -k(T)\nabla T. \tag{5}$$

Remove q from Eqs. (3) and (5), and the consequence gives

$$\begin{aligned} &\xi_1\frac{\partial T}{\partial x_1} + \xi_2\frac{\partial T}{\partial x_2} \\ &+ \tau_0\left(\begin{array}{l}\xi_1^2\frac{\partial \xi_1}{\partial x_1}\frac{\partial T}{\partial x_1} + \xi_2\frac{\partial \xi_2}{\partial x_2}\frac{\partial T}{\partial x_2} + \xi_1\frac{\partial \xi_2}{\partial x_1}\frac{\partial T}{\partial x_2} \\ + \xi_2\frac{\partial \xi_1}{\partial x_2}\frac{\partial T}{\partial x_1} + 2\xi_1\xi_2\frac{\partial^2 T}{\partial x_1 \partial x_2} + \xi_1^2\frac{\partial^2 T}{\partial x_1^2} + \xi_2^2\frac{\partial^2 T}{\partial x_2^2}\end{array}\right) \\ &- \frac{Q}{\rho c_p}\left(T - T_\infty\right) - \tau_0\frac{Q}{\rho c_p}\left(\xi_1\frac{\partial T}{\partial x_1} + \xi_2\frac{\partial T}{\partial x_2}\right) \\ &= \frac{1}{\rho c_p}\frac{\partial}{\partial \xi_2}\left(k(T)\frac{\partial T}{\partial \xi_2}\right). \end{aligned} \tag{6}$$

Boundary conditions related to this issue are

$$\begin{aligned} &\xi_1 = U_w(x_1) = U_0(x_1+b)^n,\ T = T_w, \\ &\xi_2 = 0,\ \text{at } x_2 = A\left(x_1+b\right)^{\frac{1-n}{2}}, \end{aligned} \tag{7}$$

$$\xi_1 = 0,\ T = T_0,\ \text{at } x_2 \to 0. \tag{8}$$

In this, velocity components are represented by ξ_1 and ξ_2, electrical conductivity denoted by σ, the kinematic viscosity of fluid denoted by ν, stretching velocity denoted by U_w, relaxation time represented by λ_1, velocity power index represented by n, dimensional constant represented by b, specific heat represented by c_p, density denoted by ρ, temperature denoted by T, reference velocity represented by U_0, and ambient temperature of the fluid denoted by T_∞, and the thermal conductivity is represented as

$$k(T) = k_\infty(1 + \varepsilon H_2). \tag{9}$$

Here, the ambient fluid thermal conductivity is represented as k_∞, the dimensionless temperature denoted by H_2 and the influence of thermal conductivity represented by a small parameter ε. Moreover, it was identified that if $\lambda_1 = \lambda_2 = 0$, then Oldroyd-B model is turned into a viscous fluid.

Applying the following variables,

$$\begin{aligned}
\zeta &= \sqrt{\frac{(n+1)U_0(x_1+b)^{n-1}}{2\upsilon}}x_2,\\
\psi &= \sqrt{\frac{U_0(x_1+b)^{n+1}2\upsilon}{n+1}}H_1(\zeta),\\
\xi_1 &= U_0(x_1+b)^n H_1'(\zeta),\\
\xi_2 &= -\sqrt{\frac{(n+1)\upsilon U_0(x_1+b)^{n-1}}{2}}\left(H_1(\zeta) + \zeta\frac{n-1}{n+1}H_1'(\zeta)\right),\\
H_2(\zeta) &= \frac{T-T_\infty}{T_w - T_\infty},
\end{aligned} \tag{10}$$

equation of incompressibility fulfilled with (10) and Eqs. (2) and (6) are turned into

$$\begin{aligned}
&H_1''' - \frac{2n}{n+1}H_1'^2 + H_1H_1''\\
&\quad + \beta_1\left((3n-1)H_1H_1'H_1'' - \frac{2n(n-1)}{n+1}H_1'^3 - \frac{n+1}{2}H_1^2H_1''' + \xi\frac{n-1}{2}H_1''H_1'^2\right)\\
&\quad + \beta_2\left(\frac{n-1}{2}H_1'H_1^3 + \left(\frac{3n-1}{2}\right)(H_1'')^2 - \frac{n+1}{2}H_1H_1^{iv}\right)\\
&\quad - M\left(H_1' - \beta_1\left(\frac{n+1}{2}H_1H_1'' + \xi\frac{n-1}{2}H_1'H_1''\right)\right) = 0,
\end{aligned} \tag{11}$$

$$\begin{aligned}
&\left(1+\varepsilon H_2\right)H_2'' + \varepsilon H_2'^2 + \Pr H_1H_2'\\
&\quad + \Pr\gamma\left(\frac{n-3}{2}H_1H_1'H_2' - \frac{n+1}{2}H_1^2H_2''\right)\\
&\quad - \Pr\delta_1 H_1H_2' + \frac{2}{n+1}\Pr\delta H_2 = 0.
\end{aligned} \tag{12}$$

Boundary conditions are transmitted into

$$H_1'(\alpha) = 1,\ H_1(\alpha) = \frac{\alpha(1-n)}{(1+n)},\ H_1'(\infty) \to 0, \tag{13}$$

$$H_2(\alpha) = 1,\ H_2(\infty) \to 0, \tag{14}$$

where δ_1 denotes the absorption/generation which is in thermal relaxation and is given by

$$\delta_1 = \frac{Q\tau_0}{\rho c_p}. \tag{15}$$

Also, δ denotes the heat absorption/generation, which is given as

$$\delta = \frac{Q}{\rho c_p U_0(x_1+b)^{n-1}}. \tag{16}$$

M is the magnetic field parameter, β_1 and β_2 denote Deborah numbers, and thermal relaxation parameter is denoted by γ.

$$\begin{aligned}
M &= \frac{\sigma B_0^2}{\rho U_0},\\
\beta_1 &= \lambda_1 U_0\left(x_1+b\right)^{n-1},\\
\beta_2 &= \lambda_2 U_0\left(x_1+b\right)^{n-1},\\
\gamma &= \tau_0 U_0\left(x_1+b\right)^{n-1}.
\end{aligned} \tag{17}$$

Also, Prandtl number is denoted by Pr

$$\Pr = \frac{\mu c_p}{k_\infty} \text{ and } \alpha = A\sqrt{\frac{(n+1)U_0}{2\upsilon}}. \tag{18}$$

In the above, A represents the plate surface. Additionally, by assuming the transformation

$$H_1(\zeta) = G(\zeta - \alpha) = G(\eta), H_2(\zeta) = \Theta(\zeta - \alpha) = \Theta(\eta). \tag{19}$$

And the governing non-dimensionalized equalities are transmitted by utilizing the boundary conditions. They are listed follows:

$$\begin{aligned}
&G''' + GG''' - \frac{2n}{n+1}G'^2\\
&\quad + \beta_1\left((3n-1)GG'G'' - \frac{2n(n-1)}{n+1}G'^3 - \frac{n+1}{2}G^2G''' + \eta\frac{n-1}{2}G''G'^2\right)\\
&\quad + \beta_2\left(\frac{n-1}{2}G'G^3 + \left(\frac{3n-1}{2}\right)(G'')^2 - \frac{n+1}{2}GG^{iv}\right)\\
&\quad - M\left(G' - \beta_1\left(\frac{n+1}{2}GG'' + \eta\frac{n-1}{2}G'G''\right)\right) = 0,
\end{aligned} \tag{20}$$

$$\begin{aligned}
&(1+\varepsilon\,\Theta)\Theta'' + \varepsilon\,\Theta'^2 + \Pr\,G\Theta'\\
&\quad + \Pr\gamma\left(\frac{n-3}{2}GG'\Theta' - \frac{n+1}{2}G^2\Theta''\right)\\
&\quad - \Pr\delta_1 G\,\Theta' + \frac{2}{n+1}\Pr\delta\,\Theta = 0,
\end{aligned} \tag{21}$$

$$G'(0) = 1,\ G(0) = \frac{\alpha(1-n)}{(1+n)},\ G'(\infty) = 0, \tag{22}$$

$$\Theta(0) = 1,\ \Theta(\infty) \to 0. \tag{23}$$

The local skin friction coefficient and the Nusselt number are represented as Cf_{x_1} and Nu_{x_1}, respectively. They are described as

$$Cf_{x_1} = \frac{\tau_w}{\rho U_w^2(x_1)},\ \mathrm{Nu}_{x_1} = \frac{(x_1+b)q_w}{k(T_w - T_\infty)}. \tag{24}$$

In the above terms

$$\tau_w = \mu \left.\frac{\partial \xi_1}{\partial x_2}\right|_{x_2 = A(x_1+b)^{\frac{1-n}{2}}},\ q_w = -k \left.\frac{\partial T}{\partial x_2}\right|_{x_2 = A(x_1+b)^{\frac{1-n}{2}}}. \tag{25}$$

With the help of (10) and (19), they can be transmuted as

$$(\mathrm{Re}_{x_1})^{1/2} Cf_{x_1} = \sqrt{\frac{n+1}{2}} G''(0),\ (\mathrm{Re}_{x_1})^{-1/2} \mathrm{Nu}_{x_1} = -\sqrt{\frac{n+1}{2}} \Theta'(0), \tag{26}$$

where Re_{x1} is defined as $\mathrm{Re}_{x_1} = \frac{U_w(x_1)(x_1+b)}{\upsilon}$.

Numerical solution

Oldroyd-B model equations are denoted by (20) and (21), and the corresponding boundary conditions represented by Eqs. (22) and (23) are nonlinear in behavior. The above nonlinear system is first converted as a scheme of the first-order ordinary differential equations. A computational scheme Runge–Kutta–Fehlberg (RKF) together with shooting technique is used for the solution.

Define a new format to Eqs. (20) and (21)

$$\begin{pmatrix} G \\ G' \\ G'' \\ G''' \\ G'''' \end{pmatrix} = \begin{pmatrix} Z_1 \\ Z_1' = Z_2 \\ Z_2' = Z_3 \\ Z_3' = Z_4 \\ Z_4' = Z_5 \end{pmatrix}, \begin{pmatrix} \Theta \\ \Theta' \\ \Theta' \end{pmatrix} = \begin{pmatrix} Z_6 \\ Z_6' = Z_7 \\ Z_7' = Z_8 \end{pmatrix}. \tag{27}$$

An initial value problem was obtained from the above subsequent system.

$$\beta_2\left(\frac{n+1}{2}\right)Z_4' = \begin{bmatrix} Z_4 + Z_1 Z_3 - \frac{2n}{n+1} Z_2^2 + \beta_1 \begin{pmatrix} (3n-1) Z_1 Z_2 Z_3 - \frac{2n(n-1)}{n+1} Z_2^3 \\ -\frac{n+1}{2} Z_1^2 Z_4 + \eta \frac{n-1}{2} Z_3 Z_2^2 \end{pmatrix} \\ +\beta_2\left(\frac{n-1}{2} Z_2 Z_1^3 + \frac{3n-1}{2} Z_3^2\right) + M\left(\beta_1\left(\frac{n+1}{2} Z_1 Z_3 + \eta \frac{n-1}{2} Z_2 Z_3\right) - Z_2\right) \end{bmatrix}, \tag{28}$$

$$Z_7'\left(1 + \varepsilon Z_6 - \mathrm{Pr}\ \gamma \frac{n+1}{2} Z_1^2\right) = \mathrm{Pr}\ \delta_1 Z_1 Z_7 - \frac{2}{n+1} \mathrm{Pr}\ \delta Z_6 - \varepsilon Z_7^2 - \mathrm{Pr}\ Z_1 Z_7 - \mathrm{Pr}\ \gamma \frac{n-3}{2} Z_1 Z_2 Z_7, \tag{29}$$

$$\begin{aligned} &Z_1(0) = \alpha\left(\frac{1-n}{1+n}\right), \\ &Z_2(0) = 1, \\ &Z_5(0) = 1, \\ &Z_2(\infty) = \Delta_1, \\ &Z_5(\infty) = \Delta_2, \end{aligned} \tag{30}$$

where $\Delta_i, i \le 2$, are the shooting constants. In total computations, suitable tolerance intensity is taken as 10^{-6}. To identify the exactness of the analysis, we compared skin friction coefficient values with the results published for special cases in those properties of the magnetic field that are ignored

Table 1 Observation of local skin coefficient $-G''(0)$ by using the previously published data

β_1	Abel et al. [52]	Megahed [53]	Abbasi et al. [54]	Shafique et al. [55]	Abbas-bandy et al. [56]	Present results
0	0.999962	0.999978	1.00000	1.000000	1.000000	1.000000
0.2	1.051948	1.051945	1.05189	1.051887	1.051890	1.051890
0.4	1.101850	1.101848	1.10190	1.101898	1.101903	1.101903
0.6	1.150163	1.150160	1.15014	1.150128	1.150137	1.150137
0.8	1.196692	1.196690	1.19671	1.196708	1.196711	1.196711
1.2	1.285257	1.285253	1.28536	1.285361	1.285363	1.285363
1.6	1.368641	1.368641	1.36873	1.368756	1.368758	1.368758
2.0	1.368641	1.447616	1.44781	1.447648	1.447651	1.447726

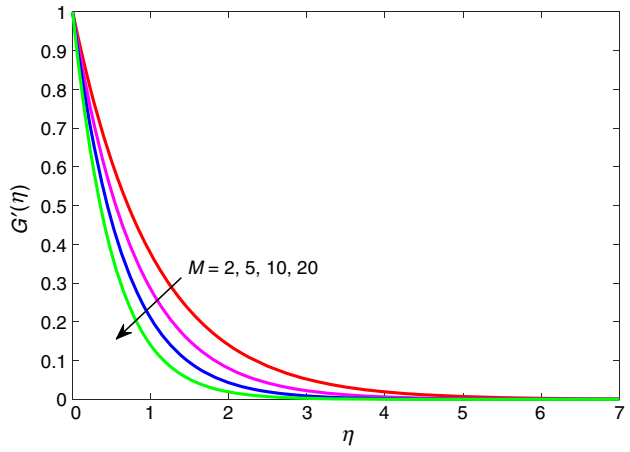

Fig. 2 Plot for velocity distribution $G^{'}(\eta)$ for distinct M

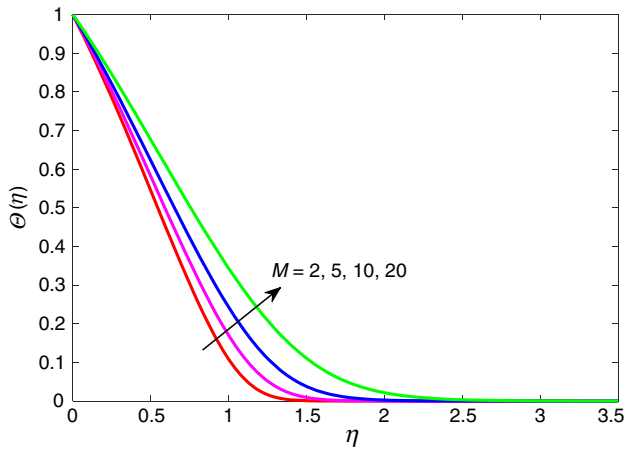

Fig. 3 Plot for temperature distribution $\Theta(\eta)$ to distinct M

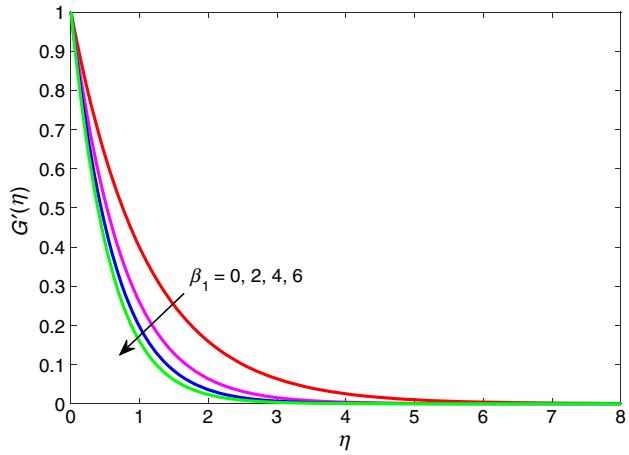

Fig. 4 Plot for velocity distribution $G^{'}(\eta)$ for distinct β_1

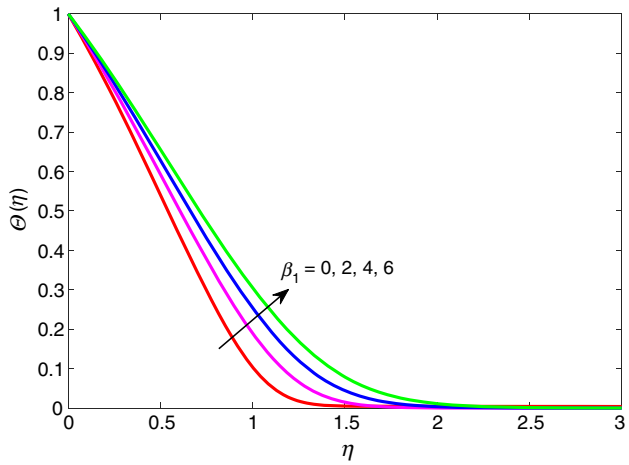

Fig. 5 Plot for temperature distribution $\Theta(\eta)$ to distinct β_1

(Table 1). Also, we identified from Table 1 that the results which are found in this paper are very similar to those of Abel et al. [52], Megahed [53], Abbasi et al. [54], Shafique et al. [55], and Abbasbandy et al. [56].

Results and discussion

The magnetic flow of Oldroyd-B type fluid is used in this paper. Impacts by relevant parameters on liquid velocity as well as temperature are validated numerically. The results obtained in this paper have much coincident with those of the previous literature.

Figures 2 and 3 represent the liquid velocity component and the temperature effects with the magnetic parameter (M) variations, respectively. Velocity component declines to the rising values of the magnetic parameter, which is shown in Fig. 2. It can be indicated as the occurrence of resistive Lorentz force throughout the appliance of the Oldroyd-B fluid. Fluid motion is decreased by using this Lorentz force inside the boundary layer, and contrary movement exists in the continuity equation. Results obtained from Fig. 2 have significant functions in polymer processing, modeling problems of injection, and so on. To the rising values of magnetic parameter (M), thermal response rises, which is pictorially represented in Fig. 3. Forced convection rises with the improvement in temperature, which lies in the Lorentz force.

Figures 4 and 5 represent the effects of velocity and temperature profiles with Deborah number β_1′s significance. Profile of velocity decreases to the more significant values of Deborah number and is observed from Fig. 4. This is the relation of relaxation time and observation time, which gives Deborah number, and by raising Deborah number, more substantial relaxation time provides additional conflict for the motion of the fluid, so velocity profile decelerates. Figures 6 and 7 represent the nature of Deborah number β_2 on velocity and temperature profiles. The velocity profile rises to the

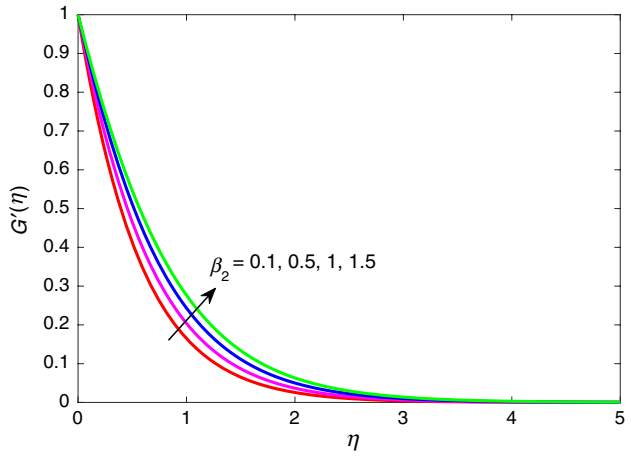

Fig. 6 Plot for velocity distribution $G^{'}(\eta)$ for distinct β_2

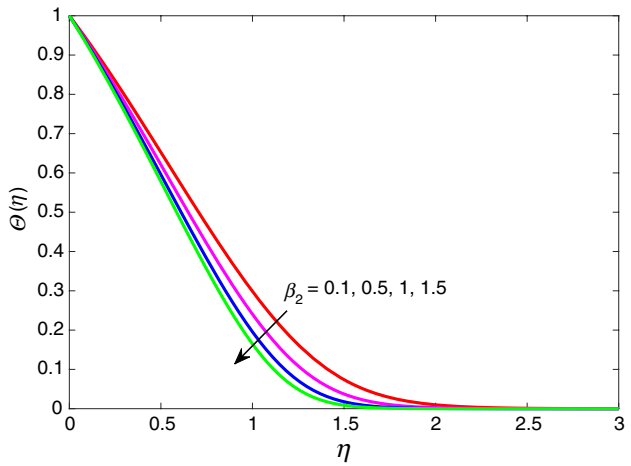

Fig. 7 Plot for temperature distribution $\Theta(\eta)$ to distinct β_2

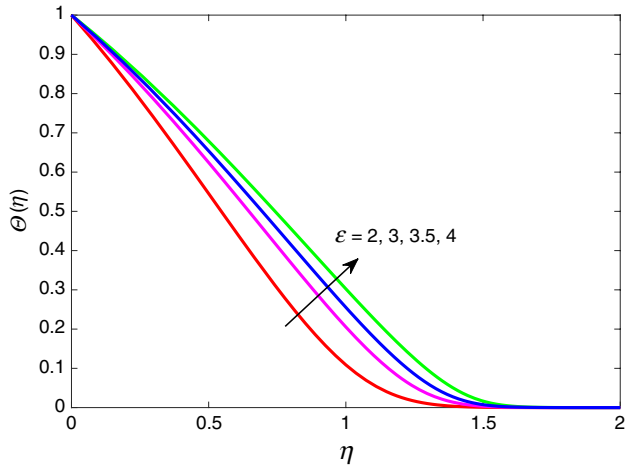

Fig. 8 Plot for temperature distribution $\Theta(\eta)$ to distinct ε

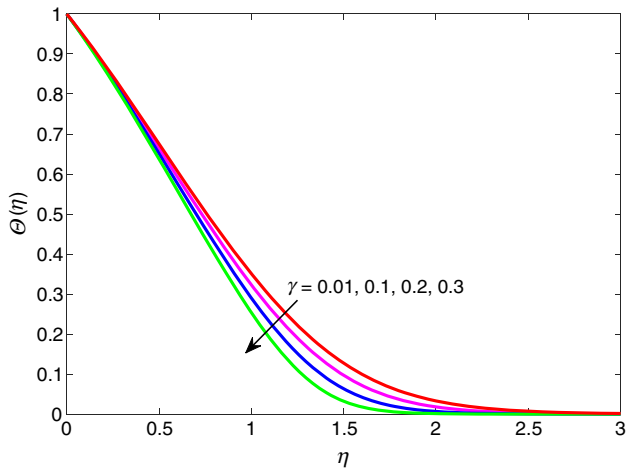

Fig. 9 Plot for temperature distribution $\Theta(\eta)$ to distinct γ

increasing values of β_2 and an associated velocity boundary-layer thickness. The temperature distribution shows opposite effects to β_1 and β_2 's rising values and is observed from Figs. 5 and 7. More substantial relaxation time and retardation time lead to higher and lower temperatures. The temperature profile is increasing and decreasing to the values of β_1 and β_2 correspondingly.

Figure 8 shows the temperature distribution increases with increasing values of E because higher thermal conductivity reaches larger values of ε. Temperature profile decreases to the more significant values of thermal relaxation parameter, which is pictorially represented in Fig. 9; because of increasing the values of thermal relaxation parameter γ, substance shows a non-conducting performance. The nature of temperature distribution with heat generation parameter δ is shown in Fig. 10. An enhancement

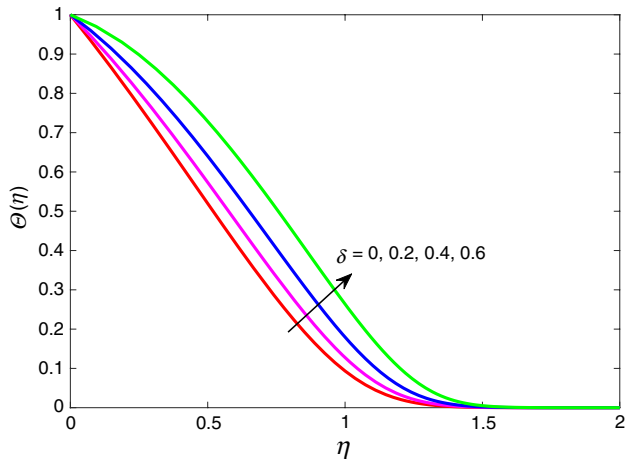

Fig. 10 Plot for temperature distribution $\Theta(\eta)$ to distinct δ

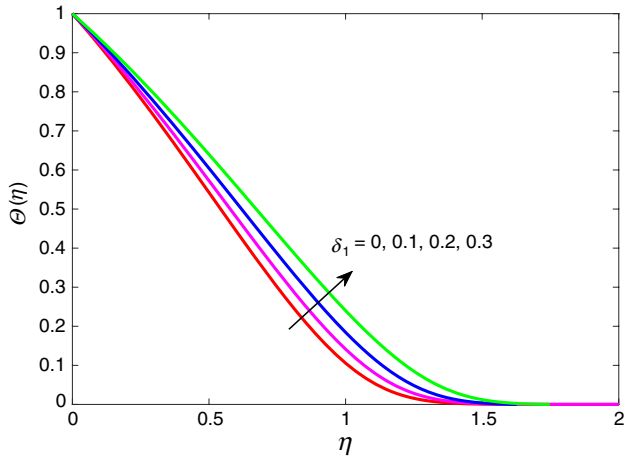

Fig. 11 Plot for temperature distribution $\Theta(\eta)$ to distinct δ_1

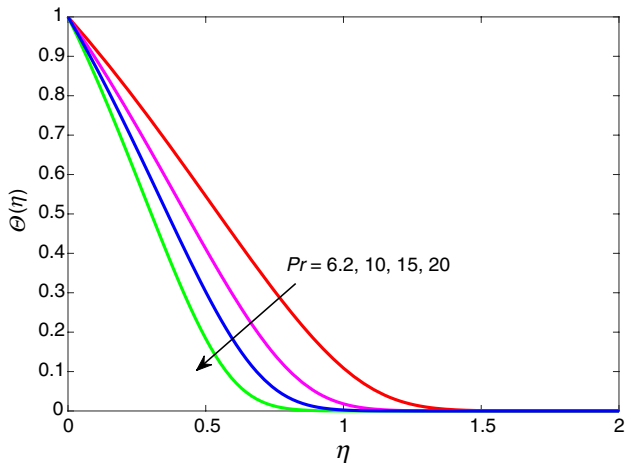

Fig. 12 Plot for temperature distribution $\Theta(\eta)$ to distinct Pr

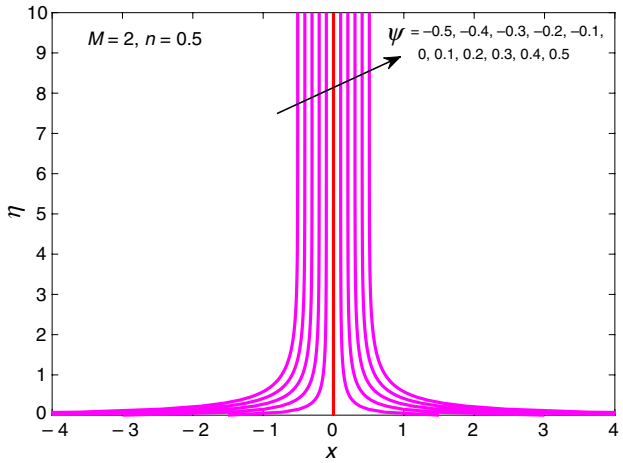

Fig. 13 Plot of streamlines for $M=2$

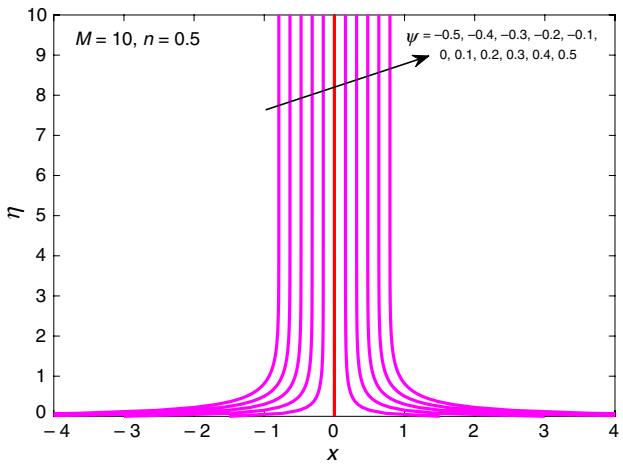

Fig. 14 Plot of streamlines for $M=10$

of temperature distribution arises by rising values of heat generation parameter and boundary-layer thickness. The behavior to the temperature profile with heat generation/absorption parameter, which is in terms of thermal relaxation δ_1, is exhibited in Fig. 11 and increases for higher values of the heat generation parameter. These outcomes are similar to those of Hayat et al. [11]. The thickness of the thermal boundary layer and temperature decrease to Prandtl number's high values, and this behavior is exhibited in Fig. 12. Increasing Pr gives lower thermal diffusivity, and it causes reducing temperature and boundary-layer thickness. Similar findings are observed in Hayat et al. [12].

The behavior of streamlines about $M=2$ and $M=10$ is exhibited in Figs. 13 and 14. It is concluded that streamlines are closed to the stagnation point $x_1=0$ for $M=2$ compared to $M=10$. Table 2 confirms that the magnitude of the local skin friction coefficient decreases as the parameter β_2 increases. The local skin friction coefficient significantly

Table 2 Local skin friction coefficient Cf_{x_1} and local Nusselt number Nu_{x_1} via $\beta_1, \beta_2, \alpha, M, \gamma, \delta$, and δ_1 when $n = 1.2$, $Pr = 6.2$, and $\varepsilon = 2$

β_1	β_2	α	M	γ	δ	δ_1	Cf_{x_1}	Nu_{x_1}
0.2	0.1	0.2	2	0.1	0.1	0.01	− 1.7972	0.62147
0.3							− 1.836	0.60817
0.4							− 1.8741	0.59496
0.5							− 1.9116	0.58184
0.6							− 1.9485	0.56883
	0.2						− 1.708	0.6375
	0.3						− 1.6331	0.65129
	0.4						− 1.5687	0.66338
	0.5						− 1.5122	0.67414
		0.4					− 1.7811	0.59154
		0.6					− 1.7652	0.56186
		0.8					− 1.7496	0.53241
		1					− 1.7342	0.50316
			4				− 2.2914	0.50358
			6				− 2.6912	0.39776
			8				− 3.0351	0.28687
			10				− 3.3407	0.10371
				0.2				0.64106
				0.3				0.66119
				0.4				0.86299
				0.5				0.97051
					0.2			0.47213
					0.24			0.39825
					0.28			0.30999
					0.3			0.25743
						0.1		0.56335
						0.2		0.49126
						0.3		0.40689
						0.4		0.29822
						0.5		0.07752

increases as β_1, α and M increases. Table 2 demonstrates a rapid increase in local Nusselt number when β_2 or γ is increased, while it decreases as the parameters $\beta_1, \alpha, M, \delta$ and δ_1 are increased. Specifically, fluid relaxation and the magnetic field harm the sheet's cooling process.

Conclusions

A numerical model is analyzed and scrutinized the consequences of the magnetic field and Cattaneo–Christov heat flux theory on Oldroyd-B fluid flow in a nonlinearly stretching sheet. By using the shooting technique, solutions of this model are developed. The primary investigations of this model are as follows:

1. Lorentz force efficiency restricts the momentum boundary layer of Oldroyd-B liquid. The momentum boundary layer is reduced and the thickness of the thermal boundary layer is reduced by the Lorentz force's proficiency.

An increase in δ and δ_1 explains an improvement in profiles of temperature and the associated thickness of the boundary layer.

An opposite behavior to the parameters β_1 and β_2 was observed in the temperature profile.

2. Streamlines are elaborated from the stagnation point for higher magnetic field strength.
3. By the strength of magnetic field intensity, local skin friction coefficient rises and heat transfer decreases.
4. Outcomes of this paper have been more important to recognize when diverging from Refs. [52–56] under exceptional cases.

The present analysis motivates future developments in melting heat transfer regimes, Joule heating, mass transfer, and thermal radiation.

References

1. Hayat T, Nadeem S. Aspects of developed heat and mass flux models on 3D flow of Eyring–Powell fluid. Res Phys. 2017;7:3910–7.
2. Ellahi R, Raza M, Vafai K. Series solutions of non-Newtonian nanofluids with Reynolds' model and Vogel's model by means of the homotopy analysis method. Math Comput Model. 2012;55:1876–91.
3. Elbashbeshy EMA, Emam TG, Abdel-Wahed MS. Three-dimensional flow over a stretching surface with thermal radiation and heat generation in the presence of chemical reaction and suction/injection. Int J Energy Technol. 2011;16:1–8.
4. Nadeem S, Hayat T, Malik MY, Rajput SA. Thermal radiations effects on the flow by an exponentially stretching surface: a series solution. Z Naturforschung. 2010;65:1–9.
5. Shenoy AV. Non-Newtonian fluid heat transfer in porous media. Adv Heat Transf. 1994;24:101–90.
6. Fourier JBJ. Theorieanalytique De Lachaleur; Paris: 1822.
7. Cattaneo C. Sulla conduzione del calore. Atti Sem Mat Fis Univ Modena. 1948;3:83–101.
8. Christov CI. On frame indifferent formulation of the Maxwell-Cattaneo model of finite speed heat conduction. Mech Res Commun. 2009;36:481–6.
9. Straughan B. Thermal convection with the Cattaneo–Christov model. Int J Heat Mass Transf. 2010;53:95–8.
10. Tibullo V, Zampoli V. A uniqueness result for the Cattaneo–Christov heat conduction model applied to incompressible fluids. Mech Res Commun. 2011;38:77–99.
11. Hayat T, Khan WA, AlsaediIjaz A, Ayub M, Ijaz Khan M. Stretched flow of Oldroyd fluid with Cattaneo–Christov heat flux. Res Phys. 2017;7:2470–6.
12. Hayat T, Ullah I, Muhammad T, Alsaedi A. Thermal and solutal stratification in mixed convection three-dimensional flow of an Oldroyd-B nanofluid. Res Phys. 2017;7:3797–805.
13. Hafeez, A., Khan, M., Ahmed, J. Thermal aspects of chemically reactive Oldroyd-B fluid flow over a rotating disk with Cattaneo–Christov heat flux theory. J Therm Anal Calorim. 2020;1–11.
14. Gireesha BJ, Ganesh Kumar K, Ramesh GK, Prasannakumara BC. Nonlinear convective heat and mass transfer of Oldroyd-B nanofluid over a stretching sheet in the presence of uniform heat source/sink. Res Phys. 2018;9:1555–63.
15. Gangadhar K, Suresh Kumar C, Ibrahim SM, Lorenzini G. Effect of viscous dissipation on upper-convected Maxwell fluid with Cattaneo–Christov heat flux model using spectral relaxation method. Defect Diffus Foru. 2018;388:146–57.
16. Menni Y, Ameur H, Inc M. Improvement of the performance of solar channels by using vortex generators and hydrogen fluid. J Therm Anal Calorim. 2020. https://doi.org/10.1007/s10973-020-10239-3.
17. Menni Y, Azzi A, Zidani C. Use of waisted triangular-shaped baffles to enhance heat transfer in a constant temperature surfaced rectangular channel. Int. J. Eng. Sci. Technol. 2017;12:3251–73.
18. Menni Y, Azzi A, Zidani C, Benyoucef B. Numerical analysis of turbulent forced—convection flow in a channel with staggered L-shaped baffles. J New Technol Mater. 2016;6:44–55.
19. Menni Y, Azzi A. Numerical analysis of thermal and aerodynamic fields in a channel with cascaded baffles. Period Polytech Mech Eng. 2018;62:16–25.
20. Menni Y, Azzi A, Didi F, Harmand S. Computational fluid dynamical analysis of new obstacle design and its impact on the heat transfer enhancement in a specific type of air flow geometry. Comput Therm Sci. 2018;10:421–47.
21. Ameur H, Menni Y. Laminar cooling of shear thinning fluids in horizontal and baffled tubes: effect of perforation in baffles. Therm Sci Eng Prog. 2019;14:100430.
22. Menni Y, Azzi A. Design and performance evaluation of air solar channels with diverse baffle structures. Comput Therm Sci. 2018;10:225–49.
23. Selimefendigil F, Oztop HF. MHD Pulsating forced convection of nanofluid over parallel plates with blocks in a channel. Int J Mech Sci. 2019;157–158:726–40.
24. Selimefendigil F, Oztop HF. Combined effects of double rotating cones and magnetic field on the mixed convection of nanofluid in a porous 3D U-bend. Int Commun Heat Mass. 2020;116:104703.
25. El-Zahar ER, Rashad AM, Seddek LF. Impacts of viscous dissipation and Brownian motion on Jeffrey nanofluid flow over an unsteady stretching surface with thermophoresis. Symmetry. 2020;12:1450.
26. Selimefendigil F, Oztop HF. Effects of local curvature and magnetic field on forced convection in a layered partly porous channel with area expansion. Int J Mech Sci. 2020;179:105696.
27. Rashad AM. Unsteady nanofluid flow over an inclined stretching surface with convective boundary condition and anisotropic slip impact. Int J Heat Technol. 2017;35:82–90.
28. Subbarayudu K, Suneetha S, Bala Anki Reddy P, Rashad AM. Framing the activation energy and binary chemical reaction on CNT's with Cattaneo–Christov heat diffusion on Maxwell nanofluid in the presence of nonlinear thermal radiation. Arab J Sci Eng. 2019;44:10313–25.
29. El-Zahar ER, Rashad AM, Seddek LF. The impact of sinusoidal surface temperature on the natural convective flow of a ferrofluid along a vertical plate. Mathematics. 2019;7:1014.
30. Reddy SRR, Bala Anki Reddy P, Rashad AM. Activation energy impact on chemically reacting Eyring–Powell nanofluid flow over a stretching cylinder. Arab J Sci Eng. 2020;45:5227–42.
31. Khan W, Idress M, Gul T, Khan MA, Bonyah E. Three non-Newtonian fluids flow considering thin film over an unsteady stretching surface with variable fluid properties. Adv Mech Eng. 2018;10:1–17.
32. Mehmood R, Rana S, Nadeem S. Transverse thermopherotic MHD Oldroyd-B fluid with Newtonian heating. Res Phys. 2018;8:686–93.
33. Iqbal K, Ahmed J, Khan M, Ahmad L, Alghamdi M. Magnetohydrodynamic thin film deposition of Carreau nanofluid over an unsteady stretching surface. Appl Phys A. 2020;126:105.
34. Eid MR. Chemical reaction effect on MHD boundary-layer flow of two-phase nanofluid model over an exponentially stretching sheet with a heat generation. J Mol Liq. 2016;220:718–25.
35. Vajravelu K, Prasad KV, Chiu-On N, Hanumesh V. MHD squeeze flow and heat transfer of a nanofluid between parallel disks with variable fluid properties and transpiration. Int J Mech Mater Eng. 2017;12:9.
36. Shit GC, Mukherjee S. MHD graphene-polydimethylsiloxane Maxwell nanofluid flow in a squeezing channel with thermal radiation effects. Appl Math Mech. 2019;40:1269–84.
37. Shah Z, Alzahrani EO, Alghamdi W, Ullah MZ, Influences of electrical MHD and Hall current on squeezing nanofluid flow inside rotating porous plates with viscous and joule dissipation effects. J Therm Anal Calorim. 2020;140:1215–27.
38. Hayat T, Muhammad T, Shehzad SA, Alsaedi A. An analytical solution for magnetohydrodynamic Oldroyd-B nanofluid flow induced by a stretching sheet with heat generation/absorption. Int J Therm Sci. 2017;111:274–88.

39. Daniel YS, Aziz ZA, Ismail Z, Salah F. Impact of thermal radiation on electrical MHD flow of nanofluid over nonlinear stretching sheet with variable thickness. Alex Eng J. 2018;57:2187–97.
40. Hayat T, Khan WA, Abbas SZ, Nadeem S, Ahmad S. Impact of induced magnetic field on second-grade nanofluid flow past a convectively heated stretching sheet. Appl Nanosci. 2020:1–9.
41. Mondal H, Almakki M, Sibanda P. Dual solutions for three-dimensional magnetohydrodynamic nanofluid flow with entropy generation. J Comput Des Eng. 2019;6:657–65.
42. Waqas H, Imran M, Muhammad T, Sait SM, Ellahi R. Numerical investigation on bioconvection flow of Oldroyd-B nanofluid with nonlinear thermal radiation and motile microorganisms over rotating disk. J Therm Anal Calorim. 2020;1–17.
43. Venkata Subba Rao M, Gangadhar K, Varma PLN. A spectral relaxation method for three-dimensional MHD flow of nanofluid flow over an exponentially stretching sheet due to convective heating: an application to solar energy. Indian J Phys. 2018;92:1577–88.
44. Sobhana Babu PR, Venkata Subba Rao M, Gangadhar K. Boundary layer flow of radioactive non-Newtonian nanofluid embedded in a porous medium over a stretched sheet using the spectral relaxation method. Mater. Today Proc. 2019;19:2672–80.
45. Gangadhar K, Narasimharao NSLV, Satyanarayana B. Thermal diffusion and viscous dissipation effects on magnetohydrodynamic heat and mass filled with TiO_2 and Al_2O_3 water based nanofluids. Comput Therm Sci. 2019;11:523–39.
46. Rashad AM. Impact of thermal radiation on MHD slip flow of a ferrofluid over a non-isothermal wedge. J Magn Magn Mater. 2017;422:25–31.
47. Ganesh Kumar K, Ramesh GK, Gireesha BJ, Rashad AM. On stretched magnetic flow of Carreau nanofluid with slip effects and nonlinear thermal radiation. Nonlinear Eng. 2019;8:340–9.
48. Reddy SRR, Bala Anki Reddy P, Rashad AM. Effectiveness of binary chemical reaction on magneto-fluid flow with Cattaneo–Christov heat flux model. Proc IMechE Part C: J. Mech Eng Sci. 2020. https://doi.org/10.1177/0954406220950347.
49. Akilu S, Narahari M. Effects of heat generation or absorption on free convection flow of a nanofluid past an isothermal inclined plate. Adv Mater Res. 2014;970:267–71.
50. Ganga B, Mohamed Yusuff Ansari S, Vishnu Ganesh N, Abdul Hakeem AK. MHD radiative boundary layer flow of nanofluid past a vertical plate with internal heat generation/absorption, viscous and ohmic dissipation effects. J Nigerian Math Soc. 2015;34:181–94.
51. Gangadhar K, Kannan T, Sakthivel G, DasaradhaRamaiah K. Unsteady free convective boundary layer flow of a nanofluid past a stretching surface using a spectral relaxation method. Int J Ambient Energy. 2020;41:609–16.
52. Abel MS, Tawade JV, Nandeppanavar MM. MHD flow and heat transfer for the upper-convected Maxwell fluid over a stretching sheet. Meccanica. 2012;47:385–93.
53. Megahed AM. Variable fluid properties and variable heat flux effects on the flow and heat transfer in a nonNewtonian Maxwell fluid over an unsteady stretching sheet with slip velocity. Chin Phys B. 2013;9:094701.
54. Abbasi FM, Mustafa M, Shehzad SA, Alhuthali MS, Hayat T. Analytical study of Cattaneo Christov heat flux model for a boundary layer flow of Oldroyd-B fluid. Chin Phys B. 2015;25:014701.
55. Shafique Z, Mustafa M, Mushtaq A. Boundary layer flow of Maxwell fluid in rotating frame with binary chemical reaction and activation energy. Res Phys. 2016;6:627–33.
56. Abbasbandy S, Mustafa M, Hayat T, Alsaedi A. Slip effects on MHD boundary layer flow of Oldroyd-B fluid past a stretching sheet: an analytic solution. J Braz Soc Mech Sci Eng. 2017;39:3389–97.